5-3-2021

Stress concentrations in a fiber reinforced composite containing functionally graded fibers

Nicholas Payne

Washington University in St. Louis

Stress concentrations in a fiber reinforced composite containing functionally graded fibers

Nicholas Payne
NSF Science and Technology Center for Engineering Mechanobiology
McKelvey School of Engineering
Washington University in St. Louis

November 28, 2020

Abstract: In this independent study project, the problem of interfacial stress concentrations was considered from the perspective of shear lag solutions. We considered a fiber encased by a coaxial matrix sheath. An applied axial load on the sheath can increase the interfacial shear stress towards the ends of the fibers within the composite. This concentration of shear stress at the ends can cause debonding and failure of the composite. Because of the shear lag phenomenon, axial stress is maximum at the half-length of the fiber and decreases towards the ends. Conversely, the transference of stresses from matrix to fiber causes the shear stress to be zero at the midpoint of the fiber and then drastically spike at the end of the fiber. This problem has been long studied through shear lag approaches. This paper studies in detail a new shear lag approach for a fiber with stiffness that varies along its length, and documents how a piecewise functionally graded fiber, linearly decreasing in stiffness from the mid-point towards the end, can alleviate this shear concentration, reducing the risk of failure. The derivation is recounted here, and the solution methods and numerical techniques I developed to solve the equations is described. A parametric study was performed in which stress fields associated with functionally graded fibers were compared to a reference case with fibers of constant stiffness. Results show that functional grading of fibers, when chosen within a specific range, can substantially alleviate stress concentrations.

Introduction and Background

Interfaces between materials are common and critical locations of failure [1-3]. This is especially true in the body, where, for example, stress concentrations at the attachment of tendon to bone are sites of frequent injury and poor healing [4-9]. A range of strategies can be observed in nature and engineering for the alleviation of such stress concentrations [10-13]. In both, macroscopic tailoring of materials and structures is observed at the interfaces between dissimilar materials [14-16]. Strategies such as interdigitation of different tissues is observed, as well as the introduction of disorder in the fibers that underlie the structural tissues of the body [17-20]. In both nature and engineering, functional grading is observed, in which the stiffnesses of tissues vary with respect to position [21-26]. This can alleviate stress concentrations [27-28]. Motivated by the observation that both fibrous structure and spatial distribution of material properties in the body appear optimized to reduce stress concentrations, we hypothesized that tailoring of the fibers themselves might be beneficial in this regard. We therefore developed a solution for the stress fields surrounding a functionally graded fiber.

The solution approach used was the approximate shear lag method [29-32]. This method enables a closed form approximation of stresses surrounding a fiber based upon approximate, simplified kinematics for the displacement field surrounding the fiber. The approach has been used extensively in engineering, and has found much utility in the study of biological attachments [33-35]. This paper studies in detail a new shear lag approach for a fiber with stiffness that varies along its length, and documents how a piecewise functionally graded fiber, linearly decreasing in stiffness from the mid-point towards the end, can alleviate this shear concentration, reducing the risk of failure. The derivation is recounted here, and the numerical techniques I developed to solve the equations is described. A parametric study was performed in which stress fields associated with functionally graded fibers were compared to a reference case with fibers of constant stiffness. Results show that functional grading of fibers, when chosen within a specific range, can substantially alleviate stress concentrations.

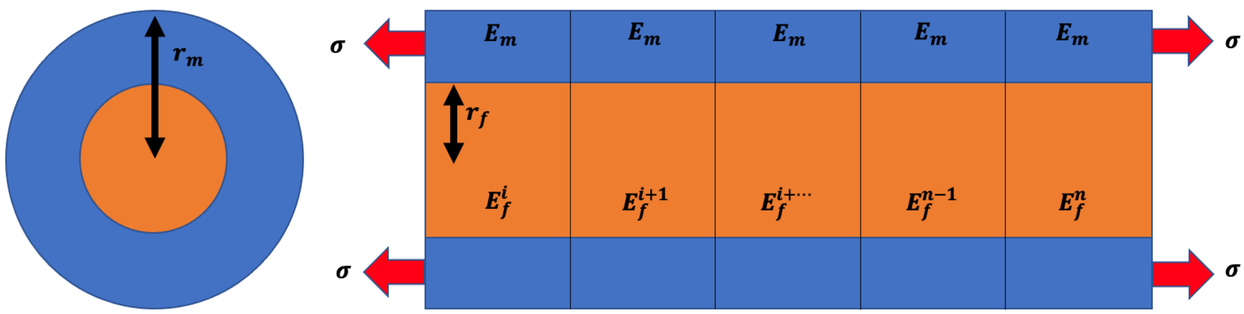

Figure 1. Model problem considered: a fiber whose stiffness varies with position, *z*.

Analysis

The shear lag analysis approach used here built from previous approaches [29-32], and was first conceived of by Victor Birman [36]. A fiber embedded in a matrix was considered (Figure 1). Rather than the standard shear lag solution, for which the fiber and matrix had identical stiffness, a case was considered in which the stiffness of the fiber varied with the axial position, z. The usual shear lag approximations were made: the fiber and matrix were treated as linearly elastic, isotropic, and perfectly bonded. The fibers were treated as being spaced in a hexagonal array so that the shear stress at the outer boundaries of cylinders that approximated this spacing could be neglected by symmetry arguments. Radial displacements and stresses were treated as negligible compared to axial displacements and stresses, so that loads transfer between the matrix and the fiber could be modeled as occurring exclusively via shear stress. Fibers were treated as very long and slender so that axial displacements, strains and stresses could be modeled as uniform across the fiber. The axial strain at the outer boundary of the cylinder of matrix enclosing the fiber was modeled as equaling the axial strain of the overall composite. The axial stresses at the ends of the fiber were treated as sufficiently small to be negligible.

With these criteria met, the piecewise solution for the axial stress $\sigma_f^j(z)$ and shear stress $\tau_f^j(z)$ in the j^{th} section of a composite with a functionally graded fiber is as follows:

$$\sigma_f^j(z) = E_f^j \varepsilon_a + A_j \sinh\left(\frac{\beta_j z}{r_f}\right) + B_j \cosh\left(\frac{\beta_j z}{r_f}\right) \tag{1}$$

$$\tau_f^j(z) = -\frac{\beta_j}{2}\left[A_j \cosh\left(\frac{\beta_j z}{r_f}\right) + B_j \sinh\left(\frac{\beta_j z}{r_f}\right)\right] \tag{2}$$

where ϵ_a is the applied strain (the mean axial strain in the composite), E_f^j is the elastic modulus of segment j, A_j and B_j are constants, β_j is the shear lag parameter defined as:

$$\beta_j^2 = \frac{2E_m}{E_f^j (1 + \nu_m) ln\left(\frac{1}{f}\right)} \tag{3}$$

in which E_m is the elastic modulus of the matrix material, ν_m is Poisson's ratio of the matrix material, and f is the volume fraction defined as:

$$f = \frac{r_f^2}{r_m^2} \tag{4}$$

where r_f is the radius of the fiber and r_m is the outer radius of the unit of fiber and matrix modeled (Figure 1). The subscripts f and m denote a relationship to either the fiber or the matrix and z is the axial distance starting from the mid-point.

To solve for the constants A_j and B_j in every piece of the composite boundary and continuity conditions were applied. The boundary conditions on the stresses were:

$$\tau_f^1(0) = 0 \tag{5}$$

$$\sigma_f^N(z = Nl_0) = 0 \tag{6}$$

in accordance with general shear lag solutions. The shear stress is zero at the midpoint and the axial stress is zero at the end of the fiber. l_0 is the length of each segment, thus Nl_0 corresponds to the very end of the composite.

The continuity conditions were the following:

$$\tau_f^j(z = jl_0) = \tau_f^{j+1}(z = jl_0) \tag{7}$$

$$\sigma_f^j(z = jl_0) = \sigma_f^{j+1}(z = jl_0) \tag{8}$$

These continuity conditions ensure that the stresses remain the same at the boundaries between the end of one segment and the beginning of the next. With N number of segments there are 2 N constants to solve for and 2 N equations.

The constants were solved for by inverting a matrix similar to the one shown below for a two-segment fiber. However, this solution holds for any integer number of segments.

$$\begin{bmatrix} 1 & 0 & 0 & 0 \\ \sinh\left(\frac{\beta_1 l_0}{r_f}\right) & \cosh\left(\frac{\beta_1 l_0}{r_f}\right) & -\sinh\left(\frac{\beta_2 l_0}{r_f}\right) & -\cosh\left(\frac{\beta_2 l_0}{r_f}\right) \\ \cosh\left(\frac{\beta_1 l_0}{r_f}\right) & \sinh\left(\frac{\beta_1 l_0}{r_f}\right) & -\frac{\beta_2}{\beta_1}\cosh\left(\frac{\beta_2 l_0}{r_f}\right) & -\frac{\beta_2}{\beta_1}\sinh\left(\frac{\beta_2 l_0}{r_f}\right) \\ 0 & 0 & \sinh\left(\frac{\beta_2 l_0}{r_f}\right) & \cosh\left(\frac{\beta_2 l_0}{r_f}\right) \end{bmatrix} \begin{bmatrix} A_1 \\ B_1 \\ A_2 \\ B_2 \end{bmatrix} = \epsilon_a \begin{bmatrix} 0 \\ E_f^2 - E_f^1 \\ 0 \\ -E_f^2 \end{bmatrix} \tag{9}$$

Code was written in MATLAB so that matrices like the one above could be quickly inverted. However, MATLAB was unable to handle the magnitude of the numbers produced by the rapid growth of the $sinh$ and $cosh$ functions. The matrix was ill-conditioned. These functions were then replaced by their exponential definitions and new equations were derived as shown below.

$$\sigma_f^j(z) = E_f^j \varepsilon_a + A_j \frac{\left(\exp(\beta_j z/r_f) - \exp(-\beta_j z/r_f)\right)}{2} + B_j \frac{\left(\exp(\beta_j z/r_f) + \exp(-\beta_j z/r_f)\right)}{2} \tag{10}$$

$$\sigma_f^j(z) = E_f^j \varepsilon_a + \frac{A_j + B_j}{2} \exp(\beta_j z/r_f) + \frac{B_j - A_j}{2} \exp(-\beta_j z/r_f) \tag{11}$$

$$\sigma_f^j(z) = E_f^j \varepsilon_a + G_j \exp\left(\frac{\beta_j z}{r_f}\right) + H_j \exp\left(-\frac{\beta_j z}{r_f}\right) \tag{12}$$

Following a similar process for the shear stresses:

$$\tau_f^j = -\frac{\beta_j}{2}\left[A_j \frac{\left(\exp(\beta_j z/r_f) + \exp(-\beta_j z/r_f)\right)}{2} + B_j \frac{\left(\exp(\beta_j z/r_f) - \exp(-\beta_j z/r_f)\right)}{2}\right] \tag{13}$$

$$\tau_f^j = -\frac{\beta_j}{2}\left[\frac{A_j + B_j}{2} \exp(\beta_j z/r_f) - \frac{B_j - A_j}{2} \exp(-\beta_j z/r_f)\right] \tag{14}$$

$$\tau_f^j = -\frac{\beta_j}{2}\left[G_j \exp(\beta_j z/r_f) - H_j \exp(-\beta_j z/r_f)\right] \tag{15}$$

The new constants, G and H in equations 14 and 15, are now the constants that need to be solved for with a matrix inversion. The boundary conditions are the same but take different forms in these equations.

$$\begin{bmatrix} 1 & -1 & 0 & 0 \\ \exp\left(\frac{\beta_1 l_0}{r_f}\right) & \exp\left(\frac{-\beta_1 l_0}{r_f}\right) & -\exp\left(\frac{\beta_2 l_0}{r_f}\right) & -\exp\left(\frac{-\beta_2 l_0}{r_f}\right) \\ \exp\left(\frac{\beta_1 l_0}{r_f}\right) & -\exp\left(\frac{-\beta_1 l_0}{r_f}\right) & -\frac{\beta_2}{\beta_1}\exp\left(\frac{\beta_2 l_0}{r_f}\right) & \frac{\beta_2}{\beta_1}\exp\left(\frac{-\beta_2 l_0}{r_f}\right) \\ 0 & 0 & \exp\left(\frac{\beta_2 l_0}{r_f}\right) & \exp\left(\frac{-\beta_2 l_0}{r_f}\right) \end{bmatrix} \begin{bmatrix} G_1 \\ H_1 \\ G_2 \\ H_2 \end{bmatrix} = \epsilon_a \begin{bmatrix} 0 \\ E_f^2 - E_f^1 \\ 0 \\ -E_f^2 \end{bmatrix} \tag{16}$$

These new equations proved to create a greatly improved matrix conditioning. For any number of segments, the matrix was able to be inverted and produce constants.

Validation and results

Once the constants were solved for, they were used in equations (14) and (15) to generate a plot of the normalized stress as a function of displacement for a fiber with a constant modulus. These plots were compared to the non-graded shear lag solution shown below:

$$\sigma_f = E_f \varepsilon_a \left[1 - \cosh\left(\frac{\beta x}{r_i}\right) \operatorname{sech}\left(\frac{\beta L}{r_i}\right)\right], \qquad \tau_i = \frac{\beta \varepsilon_a E_f}{2} \sinh\left(\frac{\beta x}{r_i}\right) \operatorname{sech}\left(\frac{\beta L}{r_i}\right) \tag{17}$$

Equations (17) were normalized and plotted as for comparison.

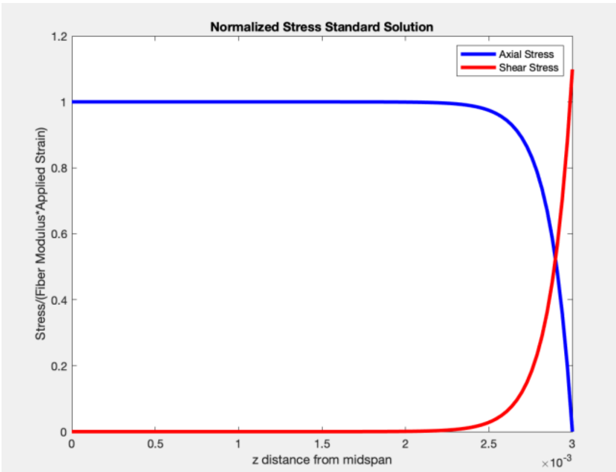

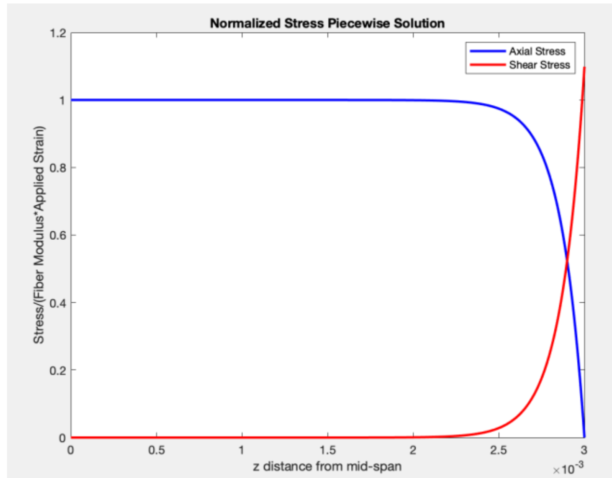

Figure 2. Comparison of Standard Shear Lag Solution to Piecewise Solution for a Constant Modulus

As shown, there is no difference in these curves. Thus, the derived piecewise solution is valid and can be used to approximate the stresses for a functionally graded fiber.

Having verified the piecewise solution, multiple curves were generated to explore the effect of a varying modulus. First the modulus was linearly increased from the midpoint of the fiber towards the end. The function for the Young's modulus gradation and various fiber and matrix properties/dimensions were: $r_f = 150\ \mu m, E_m = .3\ GPa, r_m = 190.5\ \mu m, \epsilon_a = 0.025\ L = 3000\ \mu m, N\ (num\ segments) = 100,\ E_f(j) = \left(.8 + \frac{.19W}{Nj}\right) GPa$

These parameters were used to generate the stress plots. *W* in the fiber modulus function corresponds to the curve number. Five curves were generated with *W* starting at zero for a constant modulus fiber. The subsequent curves had W values that increased by one each time (*W*=0,1,2,3,4) to create a steeper gradient. The generated curves are shown below in Figure 3.

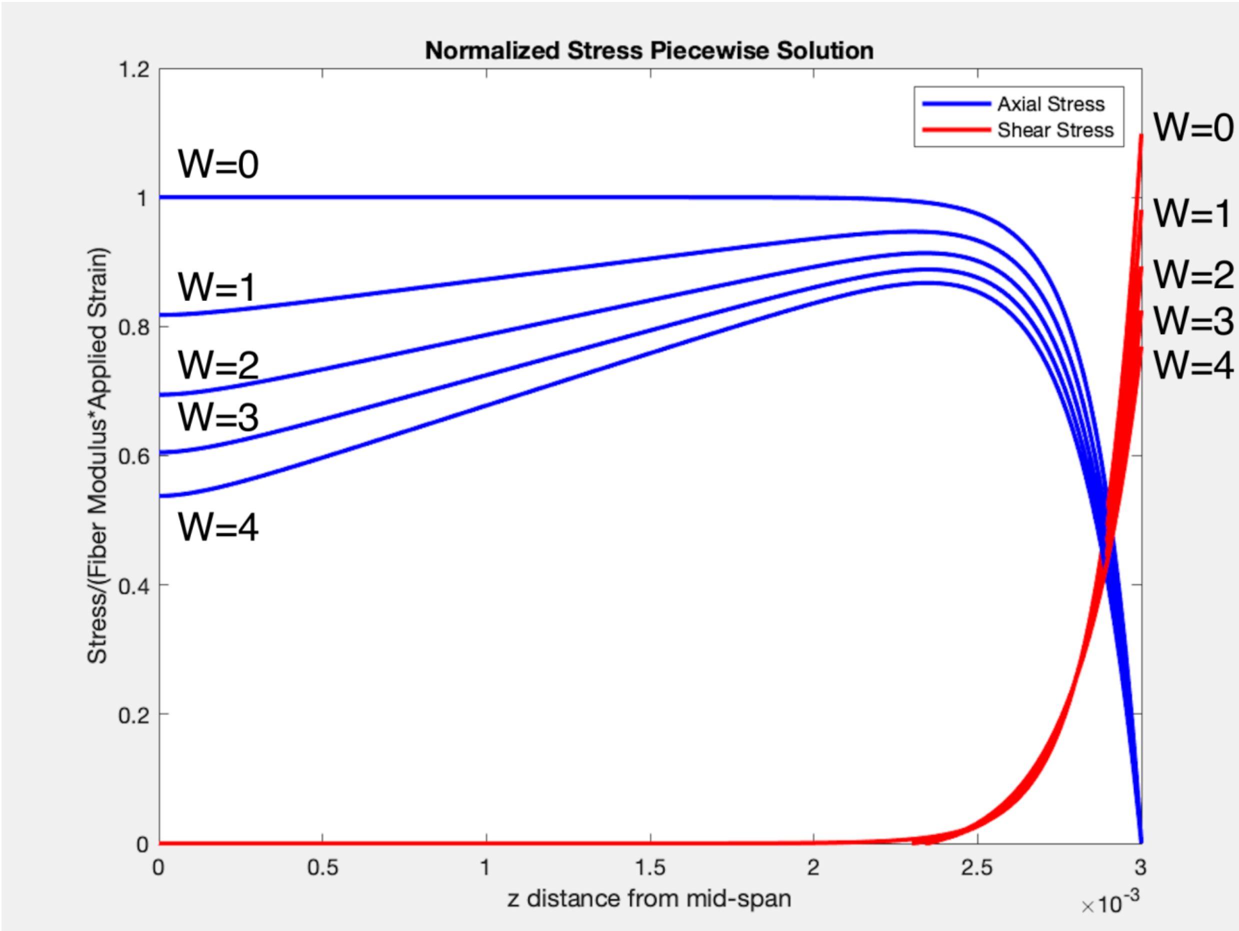

Figure 3. Stress Plot for a Fiber with a Linearly Increasing Modulus

Compared to the constant modulus solution (W=0) a slight reduction in the shear stress concentration was achieved by linearly increasing the modulus of the fiber. The steeper the gradient, the more of a reduction.

The same parameters as above were used to create a model for a fiber with a decreasing modulus where:

$$E_f(j) = \left(.8 - \frac{.19W}{Nj}\right) \text{GPa} \tag{18}$$

The results of a study for a fiber with a linearly decreasing modulus are shown below.

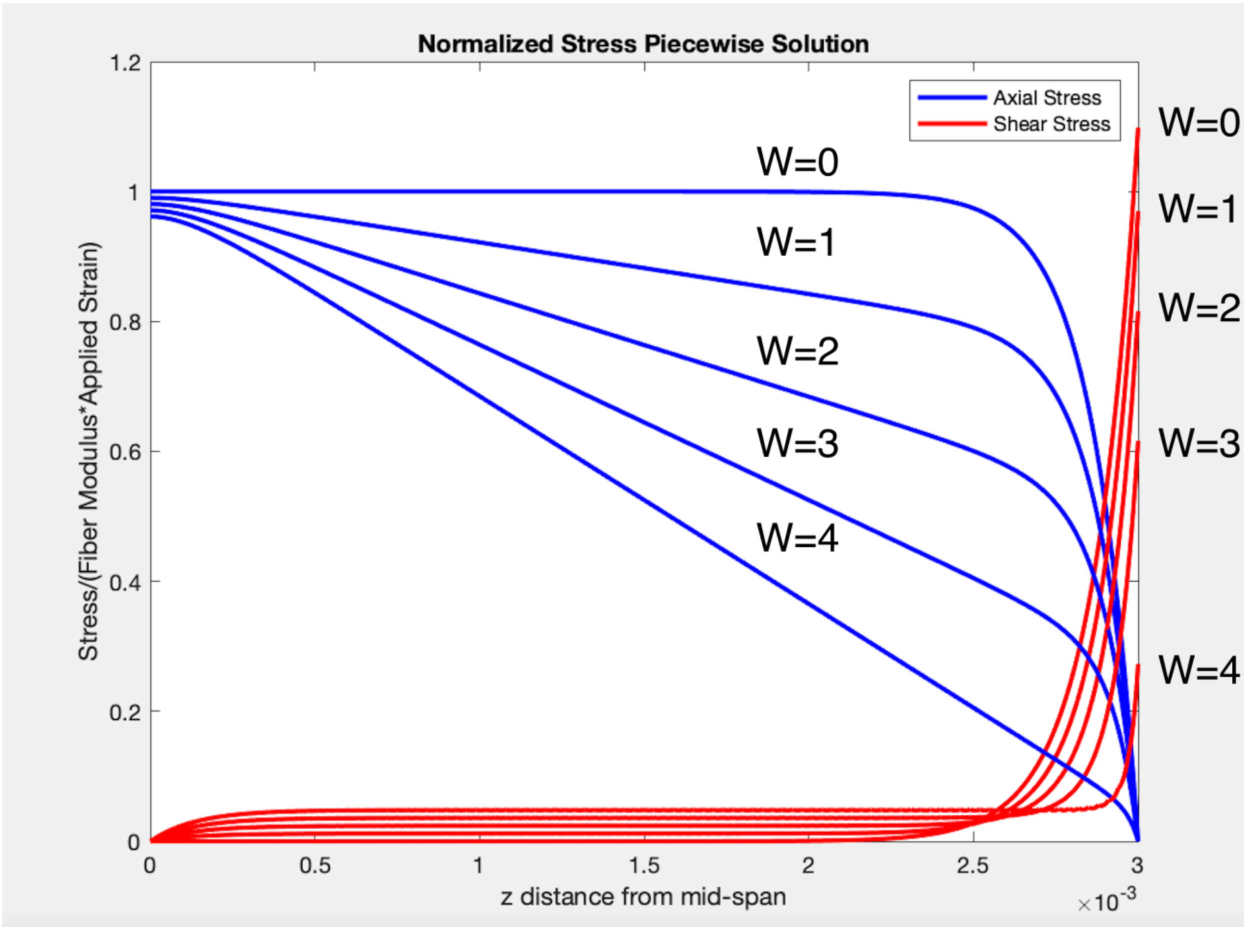

Figure 4: Stress Plot for a Fiber with a Linearly Decreasing Modulus

Compared to the constant modulus solution (W=0), a drastic reduction in the shear stress concentration was achieved as the gradient was increased.

Thus, it can be concluded that steeply decreasing the Young's Modulus of a fiber in a composite will vastly reduce the shear stress concentration in the composite, reducing the chances of debonding or failure.

Conclusion

The interfacial stress concentration that occurs in a composite can be reduced by a functional grading of the modulus in the fiber. Either increasing or decreasing the modulus will reduce this concentration but a steep decrease of the modulus towards the end of fiber yielded the greatest reduction of the concentration.

This solution can be applied to the insertion of tendon into muscle. If tendon is approximated as linearly isotropic, it can take the role of the fiber, muscle would become the matrix. As tendon enters muscle, its radius decreases as it tapers off. Therefore, the reduction in stiffness does not come from a change in modulus, rather, it comes from the tapering of the tendon. Further research is needed but this could serve to explain why the tendon-muscle connection is so strong, and better to repair it.

Acknowledgments

I thank my mentors for this independent study project, Victor Birman (Missouri University of Science and Technology) and Guy Genin (Washington University) for their guidance throughout this work. I am also grateful for helpful and informative discussions with Mikhail Golman (Columbia University) and Stavros Thomopoulos (Columbia University).

References

1. Thomopoulos, S. V. Birman and G.M. Genin, Structural Attachments and Interfaces in Biology, Springer, New York, Heidelberg, Dordrecht, London (ISBN 978-1-4614-3316-3 ISBN 978-1-4614-3317-0 (eBook)), DOI 10.1007/978-1-4614-3317-0), 2013.

2. Williams, M.L., 1952. Stress singularities resulting from various boundary conditions in angular corners of plates in extension. *Journal of applied mechanics*, *19*(4), pp.526-528.

3. Bogy, D. L., Two Edge-Bonded Elastic Wedges of Different Materials and Wedge Angles Under Surface Tractions. *J. Appl. Mech*. 1971, 38(4): 911–918

4. Mather III RC, Koenig L, Acevedo D, et al. 2013. The societal and economic value of rotator cuff repair. The Journal of bone and joint surgery American volume 95:1993.

5. Sperling JW, Cofield RH, Schleck C. 2004. Rotator cuff repair in patients fifty years of age and younger. JBJS 86:2212-2215.

6. Yamaguchi K, Ditsios K, Middleton WD, et al. 2006. The demographic and morphological features of rotator cuff disease: a comparison of asymptomatic and symptomatic shoulders. JBJS 88:1699-1704.

7. Paxton ES, Teefey SA, Dahiya N, et al. 2013. Clinical and radiographic outcomes of failed repairs of large or massive rotator cuff tears: minimum ten-year follow-up. JBJS 95:627-632.

8. Harryman D, Mack L, Wang K, et al. 1991. Repairs of the rotator cuff. Correlation of functional results with. J Bone Joint Surg Am 73:982-989.

9. Galatz LM, Ball CM, Teefey SA, et al. 2004. The outcome and repair integrity of completely arthroscopically repaired large and massive rotator cuff tears. JBJS 86:219-224.

10. L.W. Byrd and V. Birman, "The Estimate of the Effect of Z-Pins on the Strain Energy Release Rate, Fracture and Fatigue in a Composite Co-Cured Z-Pinned Double Cantilever Beam," Composite Structures, Vol. 68, pp. 53-63, 2005.

11. V. Birman and L.W. Byrd, “Effect of Z-Pins on Fracture in Composite Cocured Double Cantilever Beams” ASCE Journal of Aerospace Engineering, Vol. 18, No. 1, pp. 51-59, 2005.

12. Y. Liu, V. Birman, C. Chen, S. Thomopoulos and G.M. Genin, “Mechanisms of Bimaterial Attachment at the Interface of Tendon to Bone” ASME Journal of Engineering Materials and Technology, Vol. 133, doi:10.1115/1.4002641. January 2011.

13. S. Thomopoulos, V. Birman and G.M. Genin, “Challenges in Attaching Dissimilar Materials,” in *Structural Interfaces and Attachments in Biology*, Eds. S. Thomopoulos, V. Birman d and G.M. Genin, pp. 3-17, Springer, New York, Heidelberg, Dordrecht, London, 2013.

14. Liu, Y., Birman, V., Chen, C., Thomopoulos, S. and Genin, G.M., 2011. Mechanisms of bimaterial attachment at the interface of tendon to bone. *Journal of engineering materials and technology*, *133*(1).

15. Y.X. Liu, S. Thomopoulos, V. Birman, J.-S. Li, and G.M. Genin, “Bi-material Attachment through a Compliant Interfacial System at the Tendon-to-Bone Insertion Site,” Mechanics of Materials. Vol. 44, pp. 83-92, 2012

16. V. Birman, Y. Liu, S. Thomopoulos and G.M. Genin, “Multiscale Optimization of Joints of Dissimilar Materials in Nature and Lessons for Engineering Applications,” in *Advanced Materials Modelling for Structures*, Eds. H. Altenbach and S. Kruch, pp. 65-75, Springer-Verlag, Berlin, Heidelberg, 2013.

17. Hu, Y., Birman, V., Deymier-Black, A., Schwartz, A.G., Thomopoulos,* S. and Genin,* G.M., 2015. Stochastic interdigitation as a toughening mechanism at the interface between tendon and bone. *Biophysical Journal*, ***108***(2), pp.431-437.

18. Genin, G.M., and Thomopoulos, S., 2017. The tendon-to-bone attachment: Unification through disarray. *Nature Materials*, **16**: pp.607-608.

19. Thomopoulos, S., Marquez, J.P., Weinberger, B., Birman, V. and Genin, G.M., 2006. Collagen fiber orientation at the tendon to bone insertion and its influence on stress concentrations. *Journal of Biomechanics*, ***39***(10), pp.1842-1851.

20. S. Thomopoulos, J. Lipner, J.J. Boyle, X. Younan, V. Birman; G.M. Genin, "Toughening of Fibrous Scaffolds by Mobile Mineral Deposits," Acta Biomaterialia, Vol. 58, pp. 492-501, 2017.

21. G.M. Genin, A. Kent, V. Birman, B. Wopenka, J.D. Pasteris, P.J. Marquez, S. Thomopoulos, "Functional Grading of Mineral and Collagen in the Attachment of Tendon to Bone," Biophysical Journal, Vol. 97, pp. 976-985, 2009.

22. V. Birman and L.W. Byrd, "Functionally Graded Stitched Laminates: Illustration on the Example of a Double Cantilever Beam," ASCE Journal of Aerospace Engineering, Vol. 19, pp. 217-226, 2006.

23. V. Birman, T. Keil and S. Hosder, "Functionally Graded Materials in Engineering," in *Structural Interfaces and Attachments in Biology*, Eds. S. Thomopoulos, V. Birman and G.M. Genin, pp. 19-41, Springer, New York, Heidelberg, Dordrecht, London, 2013.

24. V. Birman and L.W. Byrd, "Modeling and Analysis of Functionally Graded Materials and Structures," Applied Mechanics Reviews, Vol. 60 (September issue), pp. 195-216, 2007.

25. F. Saadat, V. Birman, S. Thomopoulos and G.M. Genin, "Effective Elastic Properties of a Composite Containing Multiple Types of Anisotropic Ellipsoidal Inclusions, with the Application to the Attachment of Tendon to Bone," Journal of the Mechanics and Physics of Solids, Vol. 82, pp. 367-377, 2015.

26. F. Saadat, A.C. Deymier, V. Birman, S. Thomopoulos and G.M. Genin, "The Concentration of Stress at the Rotator Cuff Tendon-to-Bone Attachment Site is Conserved Across Species," Journal of the Mechanical Behavior of Biomedical Materials, Vol. 62, pp. 24-32, 2016.

27. Y. Liu, A.G. Schwartz, V. Birman, S. Thomopoulos and G.M. Genin, “Stress Amplification during Development of the Tendon-to-Bone Attachment,” Biomechanics and Modelling in Mechanobiology, doi 10.1007/s10237-013-0548-2, Vol. 13, pp. 973-983, 2014.

28. Y. Liu, S. Thomopoulos, C. Chen, V. Birman, M. Buehler and G.M. Genin, “Modeling the Mechanics of Partially Mineralized Collagen Fibrils, Fiber and Tissue,” Journal of the Royal Society. Interface 2014, Vol. 11, DOI 10.1098/rsif.2013.0835

29. V. Volkersen, Die Nietkraftverteilung in zugbeanspruchten Nievtverbindungen mit konstanten Laschenquerschnitten, Luftfahrforschung 15 (1938) 41–47.

30. H. Cox, The elasticity and strength of paper and other fibrous materials, Br. J. Appl. Phys. 3 (3) (1952) 72.

31. J.A. Nairn, On the use of shear-lag methods for analysis of stress transfer in unidirectional composites, Mech. Mater. 26 (2) (1997) 63–80.

32. J.A. Nairn, D.A. Mendels, On the use of planar shear-lag methods for stress- transfer analysis of multilayered composites, Mech. Mater. 33 (2001) 335–362.

33. S.W. Linderman, I. Kormpakis, R.H. Gelberman, V. Birman, U.G.K. Wegst, G.M. Genin and St. Thomopoulos, “Shear Lag Sutures: Improved Suture Repair Through the Use of Adhesives,” Acta Biomaterialia, Vol. 23, pp. 229-239, 2015.

34. S. Thomopoulos, S.L. Linderman, M. Golman, G.R. Thomas, V. Birman, W.N. Levine, G.M. Genin, “Enhanced Tendon-to-Bone Repair through Adhesive Films,” Acta Biomaterialia, Vol. 70, pp. 165-176, 2018.

35. I. Avgoulas, M.P.F. Sutcliffe, S.W. Linderman, V. Birman, S. Thomopoulos, and G.M. Genin, “Adhesive-Based Tendon-to-Bone Repair: Failure Modeling and Materials Selection,” Journal of the Royal Society, Interface, Vol. 16: 20180838, 2019.

36. Birman, V. Private communication.